

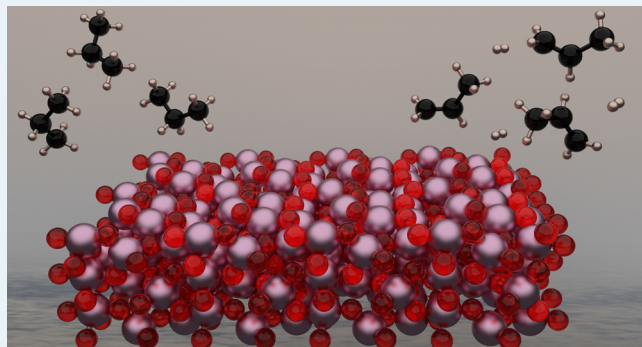
# Structure–Activity Relationships in Alkane Dehydrogenation on $\gamma\text{-Al}_2\text{O}_3$ : Site-Dependent Reactions

Mudit Dixit,<sup>1D</sup> Pavlo Kostetsky, and Giannis Mpourmpakis<sup>\*ID</sup>

Department of Chemical Engineering, University of Pittsburgh, Pittsburgh, Pennsylvania 15261, United States

 Supporting Information

**ABSTRACT:** A promising route to produce olefins, the building blocks for plastics and chemicals, is the nonoxidative dehydrogenation of alkanes on metal oxides, taking advantage of the Lewis acid–base surface functionalities of the oxides. However, how alkane dehydrogenation activity depends on the strength of surface acid–base site pairs is still elusive. In this work, we provide fundamental insights into the reaction mechanisms of propane dehydrogenation on different facets of  $\gamma\text{-Al}_2\text{O}_3$  and develop structure–activity relationships, using density functional theory calculations and first-principles molecular dynamics simulations. We identified the binding energy of dissociated  $\text{H}_2$  as an activity descriptor for alkane dehydrogenation. Interestingly, a volcano relationship between catalytic activity and dissociative  $\text{H}_2$  binding energy was discovered for propane dehydrogenation, unraveling a site-dependent catalytic behavior on  $\gamma\text{-Al}_2\text{O}_3$ , with a concerted surface mechanism being energetically preferred to a sequential one on the most active sites. We demonstrated that although surface hydration, in general, blocks strong Lewis acid–base pairs on the (110)  $\gamma\text{-Al}_2\text{O}_3$  surface, the presence of hydroxyl groups (on neighboring to strong Lewis sites) can enhance the propane dehydrogenation activity of a “defect site pair” ( $\text{Al}^{\text{III}}\text{-O}^{\text{III}}$ ) of the metastable surface. Moreover, we performed ab initio metadynamics simulations of the most active site on  $\gamma\text{-Al}_2\text{O}_3$  to examine the hydrogen formation and surface dynamics under dehydrogenation reaction conditions. Metadynamics simulations demonstrated that the poisoning of active sites by hydrogen adsorption is unlikely under experimental conditions. The developed relationships can be utilized to screen metal oxide surfaces and accelerate the discovery of active catalysts for alkane conversion to olefins.



**KEYWORDS:** density functional theory, catalyst activity, propane dehydrogenation, volcano plot, oxides, surface hydration, metadynamics

## INTRODUCTION

Light olefins are among the most important compounds used as building blocks in the chemical industry<sup>1,2</sup> for the synthesis of petrochemicals, plastics, and polymers. The gap between global demand and supply for these building-block chemicals is rapidly increasing.<sup>3</sup> Most common methods for the production of olefins include steam cracking and fluid catalytic cracking of naphtha and other petroleum products.<sup>4</sup> However, these unit operations suffer from drawbacks such as the use of nonrenewable fossil fuel resources, requirement of energy-intensive cracking processes, and low selectivity control in these reactions.<sup>1,4</sup> The challenges associated with the conventional processes for production of light olefins has directed research toward alternate synthesis methods for improvement of process economics and olefin selectivity.<sup>1,3,5,6</sup> At the same time, light alkanes are economical feedstocks, abundant in petroleum resources and shale gas. The recent dramatic increase in shale gas production has reduced the price of light alkanes, offering an excellent opportunity for the large-scale production of olefins via alkane catalytic dehydrogenation (DH).<sup>1,7,8</sup> As the C–H bonds of alkanes are more stable than

the C–C bonds, catalysts that can selectively activate the C–H bonds are highly desired.

Metal oxides, due to their inherent Lewis acidity (metal centers) and basicity (oxygen centers), can selectively activate C–H bonds of alkanes.<sup>1,9–16</sup> However, alkane DH on metal oxides requires energy-intensive operating conditions, characterized by high temperatures (500–700 °C) and low pressures. On the other hand, thermal cracking of alkanes does not occur at these operating conditions, as it requires significantly high pressures (5–70 bar).<sup>1</sup> A number of metal oxides have shown promise for nonoxidative (direct) DH of alkanes, such as  $\text{Cr}_x\text{O}_3$ ,  $\text{V}_2\text{O}_5$ ,  $\text{Ga}_2\text{O}_3$ , etc.<sup>1,9–16</sup> Notably, it has been suggested that C–H activation is the rate-limiting step for alkane DH reactions.<sup>1,17</sup>

Recently,  $\text{Al}_2\text{O}_3$  has been shown to be an active alkane DH catalyst.<sup>18</sup> The high-temperature pretreatment of  $\text{Al}_2\text{O}_3$  activates the catalyst by exposing under-coordinated surface

Received: August 30, 2018

Revised: October 17, 2018

Published: October 24, 2018



acid–base site pairs, resulting in high DH activity of  $\text{Al}_2\text{O}_3$ .<sup>18</sup> In a recent study, Valla et al. have shown that high-temperature pretreatments of  $\gamma\text{-Al}_2\text{O}_3$  generate tricoordinated Al sites, which are normally hydroxylated (poisoned) otherwise.<sup>19</sup> Sautet and co-workers studied the propane DH on  $\gamma\text{-Al}_2\text{O}_3$  (110), evaluating concerted and stepwise mechanisms for C–H activation on a single catalytic site ( $\text{Al}^{\text{III}}\text{-O}^{\text{II}}$ ).<sup>20</sup> The barrier for C–H activation of propane on clean (nonhydroxylated) catalysts was found to be lower for the stepwise pathway (25 kJ/mol) rather than for the concerted pathway (127 kJ/mol). Current industrial processes utilize  $\text{Cr}_x\text{O}_3$ -based and supported Pt-based catalysts;<sup>1,2</sup> however, both of these classes of catalysts suffer from drawbacks like the toxic nature of chromium<sup>21</sup> and high cost of precious metals. Despite significant research efforts devoted to C–H activation and DH of alkanes over the last century, there is no systematic and rational approach to screening and designing DH catalysts. Currently, DH catalysts are selected mainly by “trial and error”, and a systematic approach to guide the rational discovery of DH catalysts is highly desired.

Structure–activity relationships (SARs—correlations between catalytic activity and catalyst–reactant physicochemical properties) developed on Lewis acid oxides can provide the rational guidelines toward understanding site-dependent chemistries and designing active catalysts.<sup>22–24</sup> Many groups have investigated the oxidative C–H activation of alkanes by computational means with a focus on identifying SARs on oxides.<sup>25–29</sup> For instance, Iglesia et al. recently developed SARs for the oxidative C–H activation on oxides using reactant–catalyst properties such as C–H bond dissociation energy, hydrogen adsorption energy, and interactions between organic radicals and formed surface hydroxyl groups at transition states.<sup>29</sup> However, development of SARs for alkane DH on metal oxides is significantly underexplored, the key hurdle being a high degree of surface heterogeneity of the oxides.<sup>30</sup> Various coordination environments of metal and oxygen atoms are present on the oxides, which further increases with the different type of facets exposed on the oxide surface.<sup>31</sup> The surface coordination of metal and oxygen atoms often govern Lewis acidity and basicity of the exposed sites.<sup>32,33</sup> The Lewis acid–base functionalities of metal oxides play a key role in catalytic behavior. However, how these functionalities affect the overall alkane DH mechanisms on the different sites of the highly heterogeneous surfaces of metal oxides still remains unclear.

This work focuses on  $\gamma\text{-Al}_2\text{O}_3$ , which has a high degree of surface site heterogeneity.<sup>29,31,33</sup> Specifically, depending on the surface crystallographic plane, Al atoms can exhibit penta-coordination ( $\text{Al}^{\text{V}}$ ), tetracoordination ( $\text{Al}^{\text{IV}}$ ), or tricoordination ( $\text{Al}^{\text{III}}$ ), and the neighboring oxygen atoms can exhibit dicoordination ( $\text{O}^{\text{II}}$ ) or tricoordination ( $\text{O}^{\text{III}}$ ).<sup>33–35</sup> This high degree of surface heterogeneity on  $\gamma\text{-Al}_2\text{O}_3$  offers an excellent platform to examine the effect of surface coordination and potentially develop SARs for the conversion of alkanes to olefins. Previous studies on Lewis-acid-catalyzed alcohol dehydration to olefins were able to establish SARs for several oxide catalysts, including  $\gamma\text{-Al}_2\text{O}_3$ .<sup>23,24</sup> Interestingly, the transition states for DH of alkanes and dehydration of alcohols are structurally similar.<sup>20,23,24</sup> Based on this structural similarity of the transition states, it is plausible that SARs can be extended to the DH of alkanes.

Herein, we investigate various mechanisms of alkane DH on two nonhydroxylated low index surface facets and the

hydroxylated (110) surface of  $\gamma\text{-Al}_2\text{O}_3$  toward the development of SARs from first-principles calculations. Such relationships can aid in screening different sites of metal oxides toward C–H activation and alkane DH activity and accelerate the discovery of active alkane DH catalysts. To the best of our knowledge, this is the first demonstration of developing SARs for the efficient conversion of alkanes (through heterolytic dissociation) to olefins on metal oxides ( $\gamma\text{-Al}_2\text{O}_3$ ).

## ■ COMPUTATIONAL METHODS

Density functional theory (DFT) calculations were performed using the CP2K suite<sup>36</sup> as the implemented linear scaling construction of the Kohn–Sham matrix with robust and efficient electronic minimization makes it very scalable for large-size systems.<sup>36,37</sup> The PBE<sup>38</sup> exchange-correlation functional was used in the DFT calculations with Grimme's D3 method to account for dispersion forces,<sup>39</sup> as the incorporation of dispersion can have a significant effect on the calculated adsorption energies.<sup>40</sup> To achieve a reasonable accuracy, DZVP basis set was used in the DFT calculations for Al and the TZVP basis set for C, O, and H atoms with the Goedecker, Teter, and Hutter (GTH) pseudopotentials. A kinetic energy cutoff of 400 Ry was used for the nudged elastic band calculations;<sup>37</sup> a kinetic energy cutoff of 500 Ry was used for calculating the  $\text{H}_2$  binding energies and relative energies of hydroxylated surfaces, and a cutoff of 350 Ry was employed for the ab initio molecular dynamics (AIMD) simulations. The geometries were relaxed using the Broyden–Fletcher–Goldfarb–Shanno (BFGS) minimization algorithm until the forces converged to  $4.0 \times 10^{-4}$  E<sub>h</sub> per bohr with SCF convergence criteria of  $10^{-7}$  au ( $10^{-6}$  for AIMD). The minimum energy pathways for alkane DH were investigated using climbing image nudged elastic band (CI-NEB) calculations, and transition states were further tuned with dimer method calculations.<sup>41</sup> All of the identified transition states were verified using vibrational frequency calculations. The nonspinel model of alumina, developed by Sautet and co-workers, was used in our calculations.<sup>32,33</sup> To model (110) and (100) facets of  $\text{Al}_2\text{O}_3$ ,  $p2 \times 1$  and  $p1 \times 2$  super cells were used (Figure S1), respectively. For surface calculations, the two bottom layers were kept frozen at their corresponding bulk positions, and a vacuum space was set to 10 Å in all the calculations. The convergence of the activation barriers was performed (for both concerted and stepwise pathways on selected site pairs) with respect to the size of supercell and noted that the considered supercells were converged within 2–5 kJ/mol. The binding energy (BE) of hydrogen atoms was computed by dissociatively adsorbing hydrogen atoms on Lewis acid and Lewis base sites of the oxide surface, according to eq 1:

$$\text{BE}_{\text{H}_2} = E_{\text{surface:H}_2} - (E_{\text{H}_2} + E_{\text{surface}}) \quad (1)$$

where  $E_{\text{surface:H}_2}$  is the total energy of a dissociated  $\text{H}_2$  adsorbed on the surface and  $E_{\text{surface}}$  and  $E_{\text{H}_2}$  are total energies of the clean surface and gas-phase  $\text{H}_2$ , respectively. AIMD and metadynamics simulations were performed using the CP2K package with a time step of 0.5 fs and using the NVT ensemble. The simulation cell was equilibrated at 700 K for 4000 steps. For metadynamics simulations of  $\text{H}_2$  formation, the Gaussian bias potentials were spawned every 50 time steps (25 fs), with a height of 1.5 kcal mol<sup>-1</sup> and widths of 0.1 au along the reaction coordinate. During the metadynamics simulation, biasing potential slowly builds up until it reaches a value sufficient to cross the energy barrier. Quadratic walls were used

to avoid the sampling of nonrelevant parts of the configuration space. The free energy surface was computed after a production run of 10000 steps. Two collective variables (CVs) were defined: (i) the sum of the distance between aluminum and hydrogen and the distance between oxygen and the other hydrogen ( $CV_1 = d_{\text{Al-H}_a} + d_{\text{O-H}_b}$ ) and (ii) the distance between two hydrogen atoms ( $CV_2 = d_{\text{H}_a-\text{H}_b}$ ).

## RESULTS AND DISCUSSION

Although nonoxidative alkane DH has been studied for more than a century,<sup>1</sup> the exact reaction mechanism is still debated. The proposed mechanism for alkane DH on metal oxides is based on a Hourieti–Polanyi-type<sup>42</sup> mechanism which follows a stepwise trajectory. A limited number of studies have been devoted to the detailed mechanistic investigation of alkane DH on metal oxides.<sup>16,20,43</sup> However, several researchers have investigated alkane DH on  $\text{Cr}_x\text{O}_3$  and  $\text{Ga}_x\text{O}_3$  systems, suggesting that a stepwise mechanism dominates.<sup>1,9,16,17</sup>

In general, there are two surface mechanisms possible for alkane DH over oxide catalysts: the concerted and stepwise pathways.<sup>20</sup> The former is characterized by olefin formation in a single step, whereas the latter is characterized by sequential abstraction of hydrogen atoms from the alkane reactant. Figure 1 illustrates the steps (C–H activation and H<sub>2</sub> production) of

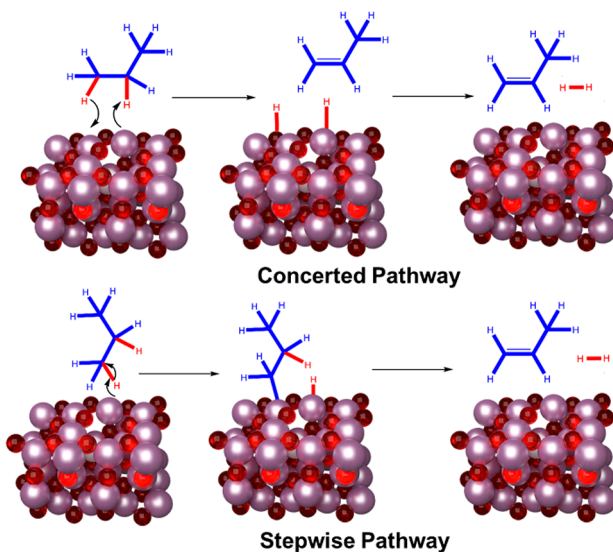


**Figure 1.** C–H activation and H<sub>2</sub> production steps of propane dehydrogenation catalyzed by  $\gamma\text{-Al}_2\text{O}_3$ . Top panel: concerted mechanism. Bottom panel: stepwise mechanism. Aluminum atoms are pictured in magenta and oxygen in red.

the concerted and stepwise pathways. In the concerted mechanism (Figure 1, top panel), two C–H bonds of the alkane break simultaneously in a concerted fashion, followed by the molecular hydrogen formation via recombination of two surface-bound hydrogen atoms. In the stepwise pathway (Figure 1, bottom panel), a single C–H bond breaks first, by the abstraction of a proton by a surface oxygen atom, with the alkyl group bonding to the surface aluminum to form a surface-bound Al-n-Alkyl species. This is followed by molecular hydrogen formation in the next step through  $\beta$ -hydrogen elimination (recombination of  $\beta$ -hydride of alkyl group and surface-bound proton).

To examine the effect of Lewis acidity and basicity on the alkane DH mechanism and activation barriers, we accounted

for both these mechanisms on the two stable, low-index surface facets of  $\gamma\text{-Al}_2\text{O}_3$ , (100) and (110), as shown in Figure 2.<sup>32,33</sup>

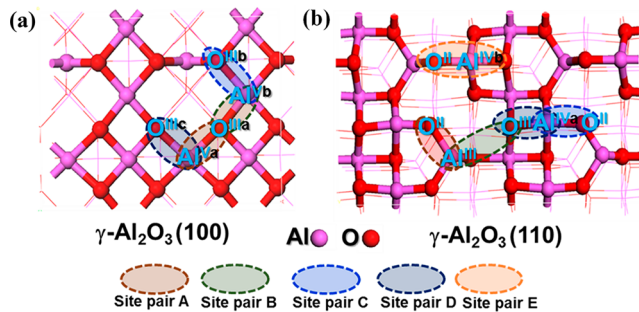


**Figure 2.** Top view of the different metal–oxygen site pairs on the (a)  $\gamma\text{-Al}_2\text{O}_3$  (100) and (b)  $\gamma\text{-Al}_2\text{O}_3$  (110) surface facets.

The two surface facets of  $\gamma\text{-Al}_2\text{O}_3$ , (100) and (110), were relaxed, and it was observed that Al atoms exhibit pentacoordination ( $\text{Al}^{\text{V}}$ ) on  $\gamma\text{-Al}_2\text{O}_3$  (100) and tetra- ( $\text{Al}^{\text{IV}}$ ) and tricoordination ( $\text{Al}^{\text{III}}$ ) on  $\gamma\text{-Al}_2\text{O}_3$  (110). Oxygen atoms were found to exhibit tricoordination ( $\text{O}^{\text{III}}$ ) on  $\gamma\text{-Al}_2\text{O}_3$  (100) and di- ( $\text{O}^{\text{II}}$ ) and tricoordination ( $\text{O}^{\text{III}}$ ) on  $\gamma\text{-Al}_2\text{O}_3$  (110).<sup>32,33</sup> Based on the coordination numbers of metal (Lewis acid) and oxygen (Lewis base) surface sites, we selected four and five symmetrically unique acid–base site pairs on (100) and (110) surface facets (highlighted in Figure 2), respectively. Specifically, the selected site pairs on  $\gamma\text{-Al}_2\text{O}_3$  (100) were  $\text{Al}^{\text{Va}}-\text{O}^{\text{IIIa}}$  (site pair A),  $\text{Al}^{\text{Vb}}-\text{O}^{\text{IIIa}}$  (site pair B),  $\text{Al}^{\text{Vb}}-\text{O}^{\text{IIIb}}$  (site pair C), and  $\text{Al}^{\text{Va}}-\text{O}^{\text{IIIc}}$  (site pair D). The selected site pairs on  $\gamma\text{-Al}_2\text{O}_3$  (110) were  $\text{Al}^{\text{III}}-\text{O}^{\text{II}}$  (site pair A),  $\text{Al}^{\text{III}}-\text{O}^{\text{III}}$  (site pair B),  $\text{Al}^{\text{IVa}}-\text{O}^{\text{II}}$  (site pair C),  $\text{Al}^{\text{IVa}}-\text{O}^{\text{III}}$  (site pair D), and  $\text{Al}^{\text{IVb}}-\text{O}^{\text{II}}$  (site pair E).

We investigated the propane DH on these site pairs for both the concerted and stepwise mechanisms.

Figure 3 shows graphical snapshots of relevant intermediates and transition states in the concerted and sequential mechanisms on the  $\text{Al}^{\text{Va}}-\text{O}^{\text{IIIa}}$  site pair of the  $\gamma\text{-Al}_2\text{O}_3$  (100) surface. For the concerted pathway (Figure 3, top panel, and Figure S2), the initial step (C–H activation) evolves through a six-membered transition state, yielding the olefin directly, with two surface-bound hydrogens on the acid–base pair. In the subsequent step (H<sub>2</sub> production), two surface-bound hydrogen atoms recombine to form molecular hydrogen. On the other hand, for the stepwise mechanism (Figure 3, bottom panel, and Figure S3), the activation of a single C–H bond yields surface-bound Al-n-propyl and hydroxyl species, with carbanionic and protic characters, respectively. In the next step, the surface-bound hydrogen and one of the  $\beta$ -hydrogen atoms of the propyl fragment combine via a six-membered transition state, resulting in the direct formation of molecular hydrogen and olefin. The graphical snapshots of the intermediates and transition states on all the selected site pairs of (100) and (110) surfaces of  $\text{Al}_2\text{O}_3$  through the concerted and stepwise mechanisms are shown in Figures S18–S37. For the stepwise pathway, we also investigated other alternative routes, including the one suggested for  $\text{Cr}_2\text{O}_3$ ,<sup>1,44,45</sup> in which the  $\beta$ -hydrogen of propane is abstracted by the metal (Al) site directly or via a 1–2 hydrogen shift. However, we note that these mechanisms exhibit significantly higher reaction barriers ( $\sim 50$ –100 kJ) higher than that of the six-membered transition state on  $\text{Al}^{\text{III}}-\text{O}^{\text{II}}$  site pair of (110) facet) and were therefore considered unlikely.

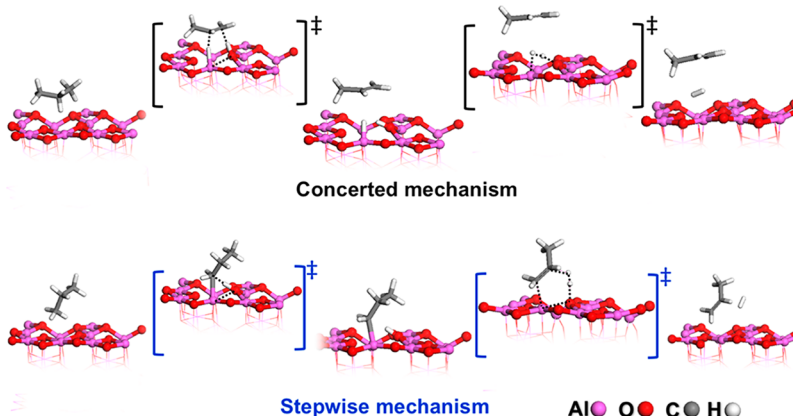


**Figure 3.** Most preferred mechanism for propane DH on  $\gamma\text{-Al}_2\text{O}_3$  (100) on  $\text{Al}^{\text{Va}}\text{-O}^{\text{IIIa}}$  site pair, transition states denoted with double daggers ( $\ddagger$ ). Top panel: concerted mechanism. Bottom panel: stepwise mechanism.

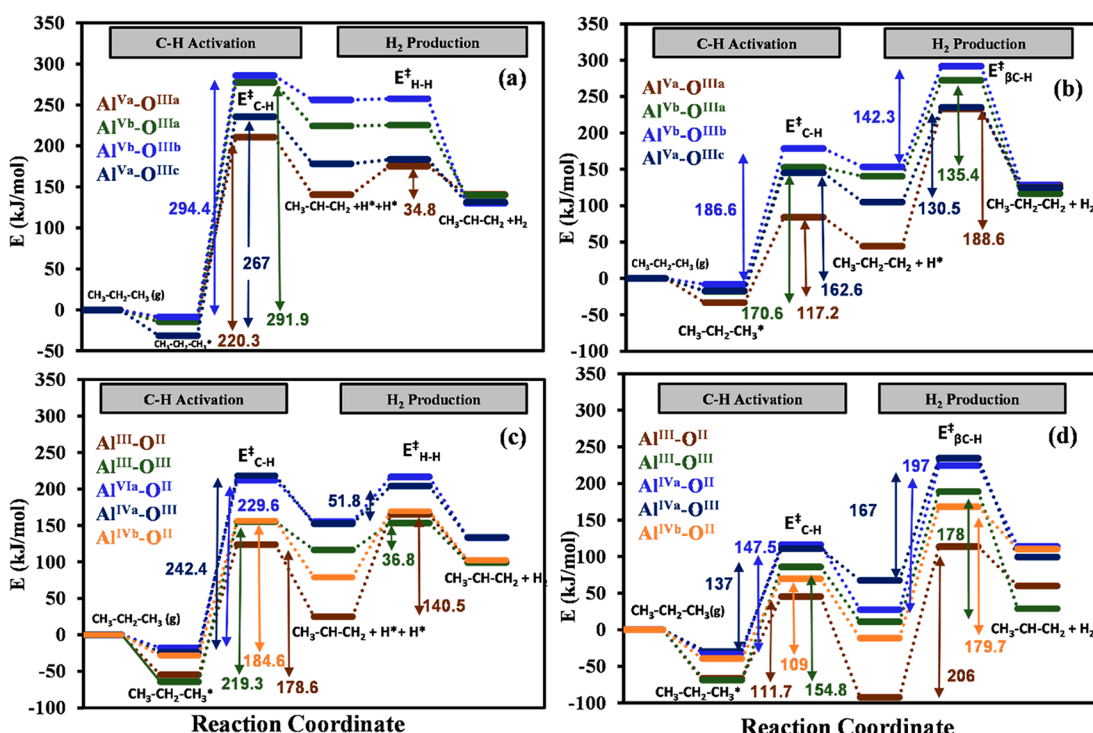


**Figure 4.** Propane DH energy profiles on  $\gamma\text{-Al}_2\text{O}_3$  (100) via (a) concerted and (b) stepwise pathways and the equivalent pathways on the (110) facet ((c) concerted and (d) stepwise). The respective site pairs are shown in Figure 2.  $E^\ddagger_{\beta\text{-C}-\text{H}}$  and  $E^\ddagger_{\text{H}-\text{H}}$  are the energies of the transition states for hydrogen production through the stepwise pathway ( $\beta\text{-C}-\text{H}$  elimination) and concerted pathway, respectively.

Now we turn our attention to the activation barriers of propane DH on different site pairs of  $\gamma\text{-Al}_2\text{O}_3$ . For both mechanisms, the physisorption of propane on both surface facets of  $\gamma\text{-Al}_2\text{O}_3$  is weakly exothermic (ca. -60 kJ/mol), characteristic of the nonpolar and inert nature of alkane molecules. Calculated binding energies of propane on the (110) facet were generally more exothermic than the binding energies on the (100) facet due to lower surface coordination of acid-base sites on the (110) facet of  $\text{Al}_2\text{O}_3$ . For the concerted mechanism, the C-H activation step is energetically demanding ( $E_a = 178\text{--}295$  kJ/mol), with the lowest activation barriers noted for the Al<sup>III</sup>-O<sup>II</sup> (178.6 kJ/mol) and Al<sup>Va</sup>-O<sup>IIIa</sup> (220.3 kJ/mol) site pairs of  $\gamma\text{-Al}_2\text{O}_3$  (110) and (100) facets, respectively. The subsequent step (H<sub>2</sub> production), through the recombination of surface-bound hydrogen atoms, was generally found to exhibit low barriers (<62 kJ/mol) on both

the surface facets of  $\text{Al}_2\text{O}_3$ . An exception was observed for the site pair with lowest surface coordination (Al<sup>III</sup>-O<sup>II</sup>) of the (110) facet of  $\text{Al}_2\text{O}_3$ , with a calculated barrier of 140.5 kJ/mol. This finding suggests the H<sub>2</sub> production could be energetically demanding on surface site pairs of a low coordination environment.

In the stepwise mechanism, we note that initial C-H activation barriers are lower ( $E_a = 111\text{--}187$  kJ/mol) than the corresponding barriers in the concerted pathway ( $E_a = 178\text{--}295$  kJ/mol) on respective site pairs. However, this trend is reversed in the H<sub>2</sub> formation step (via  $\beta$ -hydrogen elimination), where the barriers for the stepwise pathway are higher (130–206 kJ/mol) than the corresponding H<sub>2</sub> formation barriers for the concerted pathway (1–140 kJ/mol) on the respective site pairs. For the stepwise pathway on two site pairs with low coordination numbers (Al<sup>III</sup>-O<sup>II</sup> and

$\text{Al}^{\text{III}}-\text{O}^{\text{II}}$ ), the alkene remains bound with aluminum even after the  $\text{H}_2$  production step and requires additional step (alkene desorption) to complete the catalytic cycle (Figure S4). Importantly, for the concerted pathway on both (100) and (110) facets (Figure 4a,c), C–H activation was found to be the rate-limiting step (RLS) as the barriers for the C–H activation step are higher than that of the  $\text{H}_2$  production step. However, for the stepwise mechanism, on several site pairs (such as  $\text{Al}^{\text{III}}-\text{O}^{\text{II}}$ ,  $\text{Al}^{\text{III}}-\text{O}^{\text{III}}$ , and  $\text{Al}^{\text{IVb}}-\text{O}^{\text{II}}$  in Figure 4d and  $\text{Al}^{\text{Va}}-\text{O}^{\text{IIIa}}$  in Figure 4b), it was observed that  $\text{H}_2$  production is the RLS, suggesting that for alkane DH, C–H activation may not necessarily be rate-determining. In the stepwise mechanism, we cleave the terminal C–H bond initially (C–H activation step) followed by the nonterminal (secondary) C–H bond in the  $\text{H}_2$  production step (RLS) because in this step the elimination of hydrogen from a secondary C–H bond (resulting in secondary carbocation) is favorable (Figure S5) compared to that of the terminal C–H bond (formation of primary carbocation).

As noted above, significantly different C–H activation and  $\text{H}_2$  formation barriers are obtained on the site pairs with dissimilar surface coordination numbers (Lewis acidity and basicity) on both facets of  $\gamma\text{-Al}_2\text{O}_3$ . To probe the Lewis acidity (metal site) and basicity (oxygen site), we identified the dissociative  $\text{H}_2$  binding energy ( $\text{BE}_{\text{H}_2}$ ) as a reactivity descriptor for the alkane DH activation energy. The rationale behind this descriptor is (i) the Sabatier principle, where the binding energy of a single adsorbate can describe catalytic activity trends, and (ii) the heterolytically dissociated hydrogen ( $\text{H}_2 \rightarrow \text{H}^+ + \text{H}^-$ ) can probe Lewis acidity and basicity via bonding with the corresponding metal and oxygen sites. First, we computed dissociated  $\text{H}_2$  binding energies of all the different site pairs on both facets ((110) and (100)), which were then plotted against the corresponding activation barriers. Figure 5 shows the correlation between dissociated  $\text{H}_2$  binding energies and the activation barriers for the two steps (C–H activation

and  $\text{H}_2$  production) of the concerted pathway. A good correlation is retrieved between the  $\text{H}_2$  binding energy and the activation energies of the two steps for the concerted mechanism (Figure 5).

Although existent, the equivalent correlations were found to be weaker in the stepwise mechanism (Figure S6), and in the  $\text{H}_2$  production step, the  $\beta$ -hydrogen is abstracted directly from the alkyl group. As a result, the transition state involves reactant property ( $\beta$ -hydrogen abstraction directly from the propyl group), unlike the concerted mechanism where the transition state involves properties of Lewis acid (surface Al atoms) and Lewis base (surface oxygen). Interestingly, our results revealed inverse trends between the activation barriers for C–H activation and  $\text{H}_2$  production steps with respect to the  $\text{H}_2$  binding energy for both the concerted and stepwise mechanisms (Figure 5 and Figure S6). These results suggest that the site pairs with strong  $\text{H}_2$  binding (strong Lewis acid–base pair) exhibit low C–H activation barriers, whereas the sites with weak  $\text{H}_2$  binding (weak Lewis acid–base pair) exhibit low  $\text{H}_2$  production barriers.

Previously, Digne et al.<sup>32,33</sup> established that for temperatures as high as 700–950 K, the (110) facet has an OH coverage of  $\sim 5.9 \text{ OH/nm}^{-2}$  (i.e., 4  $\text{H}_2\text{O}$  molecules per  $p2 \times 1$  supercell), whereas the (100) surface is expected to be water-free under the experimental DH conditions. To study the effect of surface hydroxylation of the  $\gamma\text{-Al}_2\text{O}_3$  (110) surface on propane DH, we considered eight different hydroxylated surface configurations, where hydroxyl groups are added at different sites ( $\text{Al}^{\text{IVa}}$  and  $\text{Al}^{\text{III}}$  sites, two  $\text{Al}^{\text{III}}$  sites,  $\text{Al}^{\text{IVb}}$  and  $\text{Al}^{\text{III}}$  sites,  $\text{Al}^{\text{IVb}}$  and  $\text{Al}^{\text{IVa}}$  sites, etc.) and different surface oxygen atoms are protonated. Out of these configurations, the three most stable (Figure S8) were selected for studying propane DH. We note that the surface structure of the most stable surface configuration is identical to previously reported most stable configuration by Sautet and co-workers,<sup>46,47</sup> where both  $\text{Al}^{\text{III}}$  and  $\text{Al}^{\text{IVb}}$  sites are blocked by hydroxyl groups.

On the surface with most stable configuration, the aluminum atom of the  $\text{Al}^{\text{III}}-\text{O}^{\text{II}}$  site pair is hydroxylated and the  $\text{O}^{\text{II}}$  site is hydrogen-bonded to the hydrogen atom bound at the neighboring  $\text{O}^{\text{II}}$  site (of the  $\text{Al}^{\text{IVb}}-\text{O}^{\text{II}}$  site pair) with a short hydrogen bond distance (1.53 Å). To assess the Lewis acidity and basicity of aluminum ( $\text{Al}^{\text{III}}$ ) and oxygen ( $\text{O}^{\text{II}}$ ) atoms of this site pair (Figure S8a), we studied the dissociative molecular hydrogen binding and noted that optimization from the chemisorbed state ( $\text{H}^* + \text{H}^*$ ) results in a barrierless combination to form molecular hydrogen. Subsequently, to investigate the concerted mechanism of propane DH on this  $\text{Al}^{\text{III}}-\text{O}^{\text{II}}$  site pair, we optimized the different guesses of the final state of C–H activation and noted that surface-bound hydrogen atoms again barrierlessly combined to form molecular hydrogen (Figure S9). We also note that the C–H activation (formation of  $\text{CH}_3\text{CH}_2\text{CH}_2^* + \text{H}^*$ ) on the  $\text{Al}^{\text{III}}-\text{O}^{\text{II}}$  site pair through the stepwise pathway on this most stable hydroxylated surface is significantly endothermic (254 kJ/mol) as opposed to the exothermic (−92 kJ/mol) C–H activation ( $\text{CH}_3\text{CH}_2\text{CH}_2 + \text{H}^*$ ) on the corresponding site pair of nonhydroxylated surfaces. These results suggest that the acidity and basicity of the strong acid–base pair ( $\text{Al}^{\text{III}}-\text{O}^{\text{II}}$ ) is significantly reduced by surface hydroxylation, and this site pair is not active for the C–H activation and DH. However, with surface hydroxylation, a new site pair is created which involves the  $\text{Al}^{\text{III}}$  site and oxygen of the hydroxyl group ( $\text{Al}^{\text{III}}-\text{OH}$ ). We studied the propane DH on this site pair via the stepwise

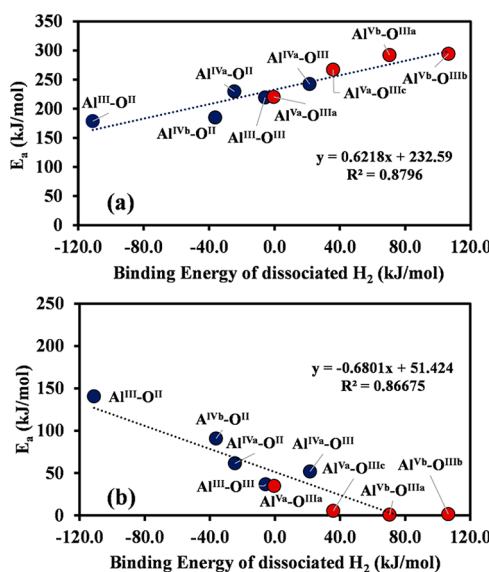


**Figure 5.** Propane DH barriers on  $\gamma\text{-Al}_2\text{O}_3$  vs dissociated  $\text{H}_2$  binding energies for (a) C–H activation and (b)  $\text{H}_2$  production steps, on the corresponding acid–base sites for the concerted mechanism. Red and blue points represent sites on (100) and (110) facets of  $\gamma\text{-Al}_2\text{O}_3$ , respectively.

pathway (**Figure S10**). It was noticed that the C–H activation barrier on the Al<sup>III</sup>–OH site pair on the most stable hydroxylated  $\gamma$ -Al<sub>2</sub>O<sub>3</sub> (110) (234.5 kJ/mol, **Figure S10**) was significantly higher than the corresponding barrier on nonhydroxylated Al<sup>III</sup>–O<sup>II</sup> site pair (~111 kJ/mol, **Figure 4d**), also exhibiting a high energetic span (289.7 kJ/mol, **Figure S10**). These results suggest that the most stable  $\gamma$ -Al<sub>2</sub>O<sub>3</sub> (110) hydroxylated surface is inactive for propane DH.

Toward rationalizing the experimentally observed activity of hydroxylated  $\gamma$ -Al<sub>2</sub>O<sub>3</sub> surfaces, in a series of seminal works, Sautet, Wischert, Copéret, and co-workers showed that surface hydration significantly influences the activity of  $\gamma$ -Al<sub>2</sub>O<sub>3</sub> (100), and high temperature pretreatment allows the formation of more active “defect” Al<sup>III</sup> sites.<sup>46,47</sup> The density of these defect sites was found to be maximum at a pretreatment temperature of 700 °C.<sup>47</sup> It was also suggested by these authors that the hydroxyl groups can increase the reactivity of a nonadjacent Al<sup>III</sup>–O<sup>III</sup> site pair by modifying the basicity of O atoms, leading to lower activation energies for H<sub>2</sub> and CH<sub>4</sub> dissociation on a metastable surface (exposed through pretreatment) when compared to the nonhydrated surface.<sup>46,47</sup> Recently Rodemerck et al.<sup>18</sup> found that the highest yield for alkane DH was obtained for a pretreatment temperature of 700 °C, suggesting that surface hydration is relevant to alkane DH, in line with previous results by Sautet et al.,<sup>46,47</sup> where a maximum reactive site density is observed at that temperature.

One of the three lowest energy hydroxylated structures, the nonreconstructed metastable structure (Digne’s model,<sup>32</sup> **Figure S8b**) was found to be 76 kJ/mol higher in energy than the most stable structure. We investigated the propane DH on Al<sup>III</sup>–O<sup>II</sup> (adjacent site pair) and Al<sup>III</sup>–O<sup>III</sup> (nonadjacent site pair) site pairs of this nonreconstructed metastable surface. It was noticed that the concerted mechanism was preferred on the Al<sup>III</sup>–O<sup>III</sup> site pair with a C–H activation barrier of 178.6 kJ/mol (**Figure S11**), which is significantly lower than that of the C–H activation barrier on Al<sup>III</sup>–O<sup>III</sup> of the nonhydrated surface (219 kJ/mol, **Figure 4c**). Accordingly, the C–H activation barrier (101.6 kJ/mol, **Figure S12**) of propane via the stepwise pathway on the metastable hydroxylated surface was found to be lower than that of the C–H activation barrier on Al<sup>III</sup>–O<sup>III</sup> site pair of the nonhydrated surface (154.8 kJ/mol, **Figure 4d**).

Even though a low barrier was obtained for the C–H activation in the stepwise pathway on Al<sup>III</sup>–O<sup>III</sup> site pair, the H<sub>2</sub> production step through  $\beta$ -hydrogen elimination was found to exhibit a high barrier (266.3 kJ/mol, **Figure S12**) on the nonreconstructed metastable hydroxylated surface. On the Al<sup>III</sup>–O<sup>II</sup> (adjacent) site pair, we found that the C–H activation barrier in the concerted pathway (233.7 kJ/mol, **Figure S13**) was significantly higher than the equivalent barrier on Al<sup>III</sup>–O<sup>III</sup> (178.6 kJ/mol, **Figure S11**) pair of the nonreconstructed metastable hydroxylated surface. These results are in line with the results obtained by Sautet and co-workers for the C–H activation of methane on the metastable surface of  $\gamma$ -Al<sub>2</sub>O<sub>3</sub> (110), where the authors found a lower C–H activation barrier on the Al<sup>III</sup>–O<sup>III</sup> compared to the Al<sup>III</sup>–O<sup>II</sup> site pair. The third hydroxylated model (**Figure S8c**) of  $\gamma$ -Al<sub>2</sub>O<sub>3</sub> (110) was found to be reconstructed (when the less basic O<sup>III</sup> site of Al<sup>Vb</sup>–O<sup>III</sup> site pair was protonated) in line with previous results by Wischert et al.<sup>46,47</sup> We note that this reconstructed metastable surface model was found to be more stable than that of the nonreconstructed model (by –47 kJ/mol) and 29 kJ/mol higher in energy than the most stable

hydroxylated configuration. We investigated the propane DH on a nonadjacent (Al<sup>III</sup>–O<sup>III</sup>) site pair of the reconstructed metastable hydroxylated surfaces through the concerted pathway and noted a C–H activation barrier of 204.4 kJ/mol (**Figure S14**), which is lower than the C–H activation barrier on the Al<sup>III</sup>–O<sup>III</sup> of the nonhydrated surface (219 kJ/mol, **Figure 4d**). In the stepwise pathway, the C–H activation barrier (86.8 kJ/mol, **Figure S15**) of propane on the Al<sup>III</sup>–O<sup>III</sup> of the metastable reconstructed hydroxylated surface was found to be significantly lower than the C–H activation barrier on Al<sup>III</sup>–O<sup>III</sup> site pair of the nonhydrated surface (154.8 kJ/mol, **Figure 4d**). However, a high barrier for H<sub>2</sub> production (240.0 kJ/mol) was noted on the Al<sup>III</sup>–O<sup>III</sup> site pair of this surface. These results clearly demonstrate that out of different site pairs studied, the Al<sup>III</sup>–O<sup>III</sup> of the metastable nonreconstructed hydroxylated surface is the most active for propane DH, and the surface hydroxylation (on neighboring positions) can increase the activity of specific site pairs. The Al<sup>III</sup> sites of the (metastable) hydroxylated surface are known to exist as “defect” sites after high temperature pretreatment of  $\gamma$ -Al<sub>2</sub>O<sub>3</sub>.<sup>46,47</sup> Recently, Rodemerck et al. showed that treating the catalyst with N<sub>2</sub>/water mixture after the high temperature (at 600 °C) kills the activity of alumina toward the DH reaction.<sup>18</sup> A possible reason for this behavior could be that treating the catalyst with N<sub>2</sub>/water mixture can block these active Lewis acid Al<sup>III</sup> defect sites which are generated by high-temperature pretreatment.

To obtain catalytic activity trends, we applied the energetic span (E-span) model of Kozuch et al.<sup>48</sup> and computed the overall turnover frequency (TOF) of the reaction at 600 °C (typical dehydrogenation temperature for Catofin dehydrogenation process).<sup>1</sup> The E-span approximation provides a simple method to calculate TOFs of multistep reactions by identifying TOF-determining transition state (TDS) and the TOF-determining intermediates (TDI). According to the E-span model, the difference of energy of TDS and TDI is the energetic span (apparent reaction barrier), and TOFs can be computed using the Arrhenius–Eyring equation (from transition state theory).<sup>48</sup> Using the E-span model, TOFs were computed for both the stepwise and concerted mechanisms for all site pairs on both facets of  $\gamma$ -Al<sub>2</sub>O<sub>3</sub> (**Table S1**).

The preference of one mechanism over the other was determined using the E-span values obtained by identifying TOF-determining intermediate and TOF-determining transition state for both mechanisms. The computed TOFs interestingly revealed that the energetically preferred propane DH mechanism changes at different site pairs of  $\gamma$ -Al<sub>2</sub>O<sub>3</sub>. We note that the concerted mechanism was found to be preferred on most of the active site pairs because the H<sub>2</sub> production step from the endothermic states (CH<sub>3</sub>CHCH<sub>2</sub> + H<sup>\*</sup> + H<sup>\*</sup>) is found to be small (<62 kJ/mol, except for Al<sup>III</sup>–O<sup>II</sup> site pair) for this mechanism, whereas in the stepwise mechanism, the H<sub>2</sub> production from the endothermic (except for Al<sup>III</sup>–O<sup>II</sup> pair) states (CH<sub>3</sub>CH<sub>2</sub>CH<sub>2</sub><sup>\*</sup> + H<sup>\*</sup>) is significantly large (>130 kJ/mol). Furthermore, to identify which pathway is preferred on a given site pair, we compared the stepwise and concerted TOFs for both mechanisms directly. By plotting the highest TOFs for a given site pair versus the dissociated H<sub>2</sub> binding energy, we identified a volcano relationship for propane dehydrogenation on  $\gamma$ -Al<sub>2</sub>O<sub>3</sub> (**Figure 6**). These results indicate that an optimal H<sub>2</sub> binding energy exists to observe high propane DH rates (TOFs). As the H<sub>2</sub> binding energy is a

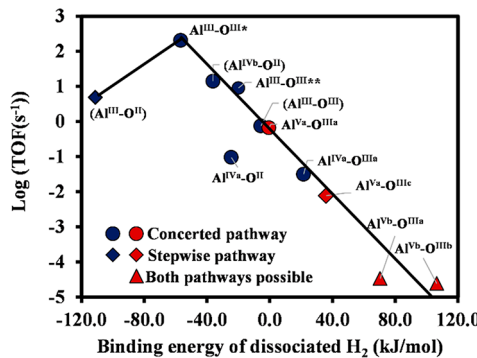


**Figure 6.** Log(TOFs) of propane DH on different site pairs for the mechanism exhibiting the highest TOFs vs  $H_2$  binding energy. Red points represent sites on the (100) and blue points on (110) facets of  $\gamma\text{-Al}_2\text{O}_3$ . Circles denote preference for the concerted, rhombus for the stepwise, and triangles for both mechanisms. The \* represents the  $\text{Al}^{\text{III}}\text{-O}^{\text{III}}$  site pair on the hydroxylated (nonreconstructed) metastable surface of  $\gamma\text{-Al}_2\text{O}_3$  (110). The \*\* indicates the  $\text{Al}^{\text{III}}\text{-O}^{\text{III}}$  site pair of the reconstructed hydroxylated surface of  $\gamma\text{-Al}_2\text{O}_3$  (110). The aluminum atoms of the site pairs shown in parentheses are expected to be hydroxylated (blocked) under experimental DH conditions.

descriptor for the strength of the Lewis acid–base pairs, this means that the active sites for alkane dehydrogenation on the surface of  $\gamma\text{-Al}_2\text{O}_3$  need to exhibit an intermediate acid–base strength. These results are in line with the Sabatier principle, stating that if the catalyst binds reactants/intermediates too strongly, it would be difficult to remove them from the catalyst surface and these sites will be eventually poisoned (i.e., high barrier to form and desorb molecular hydrogen from its dissociated state on the surface). Importantly, for the site pairs with the highest TOFs ( $\text{Al}^{\text{III}}\text{-O}^{\text{III}}$  on the hydroxylated nonreconstructed (110) facet of  $\gamma\text{-Al}_2\text{O}_3$ , located at the top of the volcano in Figure 6), the concerted mechanism was highly preferred over the stepwise mechanism. It was also noted that on two site pairs ( $\text{Al}^{\text{III}}\text{-O}^{\text{II}}$  and  $\text{Al}^{\text{V}\alpha}\text{-O}^{\text{III}c}$ ), the stepwise mechanism was found to be preferred. On two site pairs, both the concerted and stepwise mechanisms could not be distinguished in terms of activity preference (represented by triangle data markers in Figure 6). These results clearly show that the propane DH mechanism was found to be site-dependent on the (100) and (110) facets of  $\gamma\text{-Al}_2\text{O}_3$ , with both facets exhibiting surface sites with maximum dehydrogenation activity. Interestingly, on the site pair with strongest dissociated hydrogen binding energy ( $\text{Al}^{\text{III}}\text{-O}^{\text{II}}$ ), the  $H_2$  production is the TOF-determining step for the stepwise mechanism.

We note that under experimental DH conditions, several sites of the  $\gamma\text{-Al}_2\text{O}_3$  (110) surface are blocked by hydroxyl groups (Figure S8). The site pairs involving these sites are shown in parentheses in Figure 6. The DH activity of these site pairs is killed due to surface hydroxylation.

Finally, to examine the feasibility of propane DH mechanisms at experimental dehydrogenation reaction conditions, we performed AIMD simulations at 700 K (slightly lower temperature than typical dehydrogenation conditions to assess  $H_2$  production). We selected the most preferred site pairs of  $\gamma\text{-Al}_2\text{O}_3$  (points on top of volcano, Figure 6) and investigated the  $H_2$  production behavior (via the concerted mechanism). Initially, the  $H_2$ -adsorbed structure on the  $\text{Al}^{\text{III}}\text{-O}^{\text{III}}$  site of the hydroxylated nonreconstructed (110) facet was subjected to equilibration at 700 K for 4000 steps.

Subsequently, we performed ab initio metadynamics simulations to examine the event of  $H_2$  formation (Figure 7). Figure

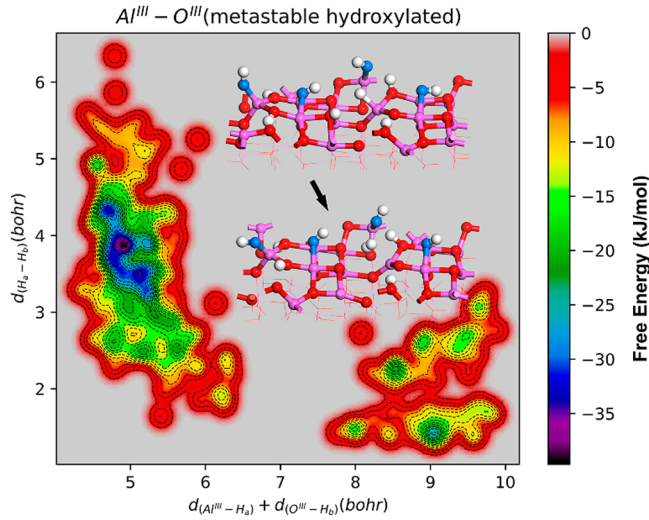


**Figure 7.** Free energy surface of metadynamics simulation (for molecular  $H_2$  formation) of hydrogen adsorbed on the  $\text{Al}^{\text{III}}\text{-O}^{\text{III}}$  site pair of the nonreconstructed hydroxylated metastable (110) facet of  $\gamma\text{-Al}_2\text{O}_3$ . Snapshots of initial and final states of metadynamics simulation are shown as insets.

7 shows the free energy surface for  $H_2$  formation on the  $\text{Al}^{\text{III}}\text{-O}^{\text{III}}$  site pair on the nonreconstructed hydroxylated (110) surface. It was noted that the free energy barrier for  $H_2$  production was found to be 39.78 kJ/mol (Figure 7) at 700 K, which can be accessible at typical dehydrogenation temperatures. These results further solidify that out of the different surface sites studied, the most active one for propane DH reactions is the  $\text{Al}^{\text{III}}\text{-O}^{\text{III}}$  on the hydroxylated nonreconstructed (110) facets of  $\gamma\text{-Al}_2\text{O}_3$ .

Additionally, we also investigated the  $H_2$  production behavior (via the concerted mechanism) on  $\text{Al}^{\text{III}}\text{-O}^{\text{III}}$  and  $\text{Al}^{\text{V}\alpha}\text{-O}^{\text{III}}$  site pairs of nonhydroxylated (110) and (100) using metadynamics simulations (Figure S7). Interestingly, it was noticed that the structure with hydrogen adsorbed on the  $\text{Al}^{\text{III}}\text{-O}^{\text{III}}$  of the nonhydroxylated (110) facet undergoes severe reconstruction, leading to a change in the coordination environment of  $\text{Al}^{\text{III}}$  and  $\text{O}^{\text{III}}$  sites after equilibration (inset of Figure S7b). However, the computed free energy barrier using metadynamics simulations (<20 kJ/mol) suggested that the hydrogen formation on  $\text{Al}^{\text{III}}\text{-O}^{\text{III}}$  and  $\text{Al}^{\text{V}\alpha}\text{-O}^{\text{III}a}$  site pairs of nonhydroxylated surfaces is feasible under experimental dehydrogenation temperatures.

## CONCLUSIONS

In this work, we applied periodic DFT calculations to investigate the propane DH on nonhydroxylated (100) and (110) and hydroxylated (110) facets of  $\gamma\text{-Al}_2\text{O}_3$  by accounting for two different DH mechanisms, concerted and stepwise. Our calculations revealed that the DH mechanism changes on the different surface sites (site-dependent mechanism), and that the most active sites for propane DH favor the concerted pathway. Interestingly, we demonstrate that the C–H activation is not necessarily the rate-limiting step for alkane DH on  $\gamma\text{-Al}_2\text{O}_3$ . Furthermore, we identified the dissociative  $H_2$  binding energy as a DH activation energy descriptor, which accounts for the strength of Lewis acid/base site pairs on the

catalyst surface. Based on this descriptor, we developed structure–activity relationships for alkane dehydrogenation that take into consideration surface acid/base properties of the oxide. We revealed a volcano relationship between the calculated propane DH TOFs and the dissociative H<sub>2</sub> binding energy. With the dissociative hydrogen binding energy governing the alkane DH activity, we further performed AIMD simulations to address the feasibility of hydrogen formation and surface dynamics of three selected sites including the most active site (Al<sup>III</sup>–O<sup>III</sup>) of hydroxylated metastable γ-Al<sub>2</sub>O<sub>3</sub> (110). Our AIMD results further verified that these sites will not be poisoned by hydrogen adsorption under experimental conditions. Finally, the developed activity relationships can aid in screening various metal oxides toward the discovery of active DH catalysts.

## ■ ASSOCIATED CONTENT

### § Supporting Information

The Supporting Information is available free of charge on the ACS Publications website at DOI: [10.1021/acscatal.8b03484](https://doi.org/10.1021/acscatal.8b03484).

Structure of surface facets of γ-Al<sub>2</sub>O<sub>3</sub>; plot of activation energy vs H<sub>2</sub> binding energy; structures of transition states and intermediates; propane DH energy profiles on γ-Al<sub>2</sub>O<sub>3</sub> (110) via stepwise pathway; propane DH energy profiles on different site pairs of hydroxylated (110) surfaces; graphical snapshots of the intermediates and transition states on all the selected site pairs of (100) and (110) surface of Al<sub>2</sub>O<sub>3</sub> through the concerted and stepwise mechanisms; Cartesian coordinates and graphical snapshots of relevant DFT structures ([PDF](#))

## ■ AUTHOR INFORMATION

### Corresponding Author

\*E-mail: [gmpourmp@pitt.edu](mailto:gmpourmp@pitt.edu).

### ORCID

Mudit Dixit: [0000-0001-9456-7806](https://orcid.org/0000-0001-9456-7806)

Giannis Mpourmpakis: [0000-0002-3063-0607](https://orcid.org/0000-0002-3063-0607)

### Notes

The authors declare no competing financial interest.

## ■ ACKNOWLEDGMENTS

Acknowledgment is made to the Donors of the American Chemical Society Petroleum Research Fund (ACS-PRF, 56989-DNIS) for support of this research. Computational support was provided by the Center for Research Computing at the University of Pittsburgh, and the Extreme Science and Engineering Discovery Environment, which is supported by the NSF (ACI-1053575).

## ■ REFERENCES

- (1) Sattler, J. J.; Ruiz-Martinez, J.; Santillan-Jimenez, E.; Weckhuysen, B. M. Catalytic Dehydrogenation of Light Alkanes on Metals and Metal Oxides. *Chem. Rev.* **2014**, *114*, 10613–10653.
- (2) Weckhuysen, B. M.; Schoonheydt, R. A. Alkane Dehydrogenation over Supported Chromium Oxide Catalysts. *Catal. Today* **1999**, *51*, 223–232.
- (3) Amghizar, I.; Vandewalle, L. A.; Van Geem, K. M.; Marin, G. B. New Trends in Olefin Production. *Engineering* **2017**, *3*, 171–178.
- (4) Sadrameli, S. M. Thermal/Catalytic Cracking of Hydrocarbons for the Production of Plefins: A State-of-the-art Review I: Thermal Cracking Review. *Fuel* **2015**, *140*, 102–115.
- (5) Zacharopoulou, V.; Lemonidou, A. Olefins from Biomass Intermediates: A Review. *Catalysts* **2018**, *8*, 2.
- (6) Hu, P.; Lang, W.-Z.; Yan, X.; Chen, X.-F.; Guo, Y.-J. Vanadium-doped porous silica materials with high catalytic activity and stability for propane dehydrogenation reaction. *Appl. Catal., A* **2018**, *553*, 65–73.
- (7) Otroshchenko, T. P.; Kondratenko, V. A.; Rodemerck, U.; Linke, D.; Kondratenko, E. V. Non-Oxidative Dehydrogenation of Propane, n-butane, and isobutane over Bulk ZrO<sub>2</sub>-based Catalysts: Effect of Dopant on the Active Site and Pathways of Product Formation. *Catal. Sci. Technol.* **2017**, *7*, 4499–4510.
- (8) Cavani, F.; Trifirò, F. The Oxidative Dehydrogenation of Ethane and Propane as an Alternative Way for the Production of Light Olefins. *Catal. Today* **1995**, *24*, 307–313.
- (9) Coperet, C. C-H Bond Activation and Organometallic Intermediates on Isolated Metal Centers on Oxide Surfaces. *Chem. Rev.* **2010**, *110*, 656–680.
- (10) Banares, M. A. Supported Metal Oxide and Other Catalysts for Ethane Conversion: a Review. *Catal. Today* **1999**, *51*, 319–348.
- (11) McFarland, E. W.; Metiu, H. Catalysis by Doped Oxides. *Chem. Rev.* **2013**, *113*, 4391–4427.
- (12) Hargreaves, J. S. J.; Hutchings, G. J.; Joyner, R. W.; Taylor, S. H. A Study of the Methane-Deuterium Exchange Reaction over a Range of Metal Oxides. *Appl. Catal., A* **2002**, *227*, 191–200.
- (13) Michorczyk, P.; Ogonowski, J. Dehydrogenation of Propane in the Presence of Carbon Dioxide Over Oxide-Based Catalysts. *React. Kinet. Catal. Lett.* **2003**, *78*, 41–47.
- (14) Nakagawa, K.; Okamura, M.; Ikenaga, N.; Suzuki, T.; Kobayashi, T. Dehydrogenation of Ethane over Gallium Oxide in The Presence of Carbon Dioxide. *Chem. Commun.* **1998**, 1025–1026.
- (15) Kazansky, V. B.; Subbotina, I. R.; Pronin, A. A.; Schlogl, R.; Jentoft, F. C. Unusual Infrared Spectrum of Ethane Adsorbed by Gallium Oxide. *J. Phys. Chem. B* **2006**, *110*, 7975–7978.
- (16) Liu, Y.; Li, Z. H.; Lu, J.; Fan, K.-N. Periodic Density Functional Theory Study of Propane Dehydrogenation over Perfect Ga<sub>2</sub>O<sub>3</sub>(100) Surface. *J. Phys. Chem. C* **2008**, *112*, 20382–20392.
- (17) Lillehaug, S.; Børve, K. J.; Sierka, M.; Sauer, J. Catalytic Dehydrogenation of Ethane over Mononuclear Cr(III) Surface Sites on Silica. part I. C—H Activation by σ-bond Metathesis. *J. Phys. Org. Chem.* **2004**, *17*, 990–1006.
- (18) Rodemerck, U.; Kondratenko, E. V.; Otroshchenko, T.; Linke, D. Unexpectedly High Activity of Bare Alumina for Non-Oxidative Isobutane Dehydrogenation. *Chem. Commun.* **2016**, *52*, 12222–12225.
- (19) Valla, M.; Wischert, R.; Comas-Vives, A.; Conley, M. P.; Verel, R.; Copéret, C.; Sautet, P. Role of Tricoordinate Al Sites in CH<sub>3</sub>ReO<sub>3</sub>/Al<sub>2</sub>O<sub>3</sub> Olefin Metathesis Catalysts. *J. Am. Chem. Soc.* **2016**, *138*, 6774–6785.
- (20) Joubert, J.; Delbecq, F.; Sautet, P. Alkane Metathesis by a Tungsten Carbyne Complex Grafted on Gamma Alumina: Is There a Direct Chemical Role of the Support? *J. Catal.* **2007**, *251*, 507–513.
- (21) Norseth, T. The Carcinogenicity of Chromium. *Environ. Health Perspect.* **1981**, *40*, 121–130.
- (22) Wachs, I. E.; Weckhuysen, B. M. Structure and Reactivity of Surface Vanadium Oxide Species on Oxide Supports. *Appl. Catal., A* **1997**, *157*, 67–90.
- (23) Kostetskyy, P.; Yu, J.; Gorte, R. J.; Mpourmpakis, G. Structure-Activity Relationships on Metal-Oxides: Alcohol Dehydration. *Catal. Sci. Technol.* **2014**, *4*, 3861–3869.
- (24) Kostetskyy, P.; Mpourmpakis, G. Structure-Activity Relationships in the Production of Olefins from Alcohols and Ethers: a First-Principles Theoretical Study. *Catal. Sci. Technol.* **2015**, *5*, 4547–4555.
- (25) Latimer, A. A.; Aljama, H.; Kakakhani, A.; Yoo, J. S.; Kulkarni, A.; Tsai, C.; Garcia-Melchor, M.; Abild-Pedersen, F.; Norskov, J. K. Mechanistic Insights into Heterogeneous Methane Activation. *Phys. Chem. Chem. Phys.* **2017**, *19*, 3575–3581.
- (26) Latimer, A. A.; Kulkarni, A. R.; Aljama, H.; Montoya, J. H.; Yoo, J. S.; Tsai, C.; Abild-Pedersen, F.; Studt, F.; Norskov, J. K.

- Understanding trends in C–H bond activation in heterogeneous catalysis. *Nat. Mater.* **2017**, *16*, 225.
- (27) Aljama, H.; Nørskov, J. K.; Abild-Pedersen, F. Theoretical Insights into Methane C–H Bond Activation on Alkaline Metal Oxides. *J. Phys. Chem. C* **2017**, *121*, 16440–16446.
- (28) Fung, V.; Tao, F. F.; Jiang, D.-e. General Structure–Reactivity Relationship for Oxygen on Transition-Metal Oxides. *J. Phys. Chem. Lett.* **2017**, *8*, 2206–2211.
- (29) Deshlahra, P.; Iglesia, E. Reactivity and Selectivity Descriptors for the Activation of C–H Bonds in Hydrocarbons and Oxygenates on Metal Oxides. *J. Phys. Chem. C* **2016**, *120*, 16741–16760.
- (30) Bell, A. T. The Impact of Nanoscience on Heterogeneous Catalysis. *Science* **2003**, *299*, 1688.
- (31) Calle-Vallejo, F.; Loffreda, D.; Koper, M. T. M.; Sautet, P. Introducing Structural Sensitivity into Adsorption–Energy Scaling Relations by Means of Coordination Numbers. *Nat. Chem.* **2015**, *7*, 403.
- (32) Digne, M.; Sautet, P.; Raybaud, P.; Euzen, P.; Toulhoat, H. Hydroxyl Groups on  $\gamma$ -Alumina Surfaces: A DFT Study. *J. Catal.* **2002**, *211*, 1–5.
- (33) Digne, M.; Sautet, P.; Raybaud, P.; Euzen, P.; Toulhoat, H. Use of DFT to achieve a rational understanding of acid–basic properties of  $\gamma$ -alumina surfaces. *J. Catal.* **2004**, *226*, 54–68.
- (34) Roy, S.; Mpourmpakis, G.; Hong, D.-Y.; Vlachos, D. G.; Bhan, A.; Gorte, R. J. Mechanistic Study of Alcohol Dehydration on  $\gamma$ -Al<sub>2</sub>O<sub>3</sub>. *ACS Catal.* **2012**, *2*, 1846–1853.
- (35) Christiansen, M. A.; Mpourmpakis, G.; Vlachos, D. G. Density Functional Theory-Computed Mechanisms of Ethylene and Diethyl Ether Formation from Ethanol on  $\gamma$ -Al<sub>2</sub>O<sub>3</sub>(100). *ACS Catal.* **2013**, *3*, 1965–1975.
- (36) VandeVondele, J.; Krack, M.; Mohamed, F.; Parrinello, M.; Chassaing, T.; Hutter, J. Quickstep: Fast and Accurate Density Functional Calculations Using a Mixed Gaussian and Plane Waves Approach. *Comput. Phys. Commun.* **2005**, *167*, 103–128.
- (37) Bethune, I.; Reid, F.; Lazzaro, A. CP2K Performance from Cray XT3 to XC30. Cray User Group, Lugano, Switzerland, May 6–8, 2014.
- (38) Perdew, J. P.; Burke, K.; Ernzerhof, M. Generalized Gradient Approximation Made Simple. *Phys. Rev. Lett.* **1996**, *77*, 3865–3868.
- (39) Grimme, S. Semiempirical GGA-type Density Functional Constructed With a Long-Range Dispersion Correction. *J. Comput. Chem.* **2006**, *27*, 1787–1799.
- (40) Gautier, S.; Steinmann, S. N.; Michel, C.; Fleurat-Lessard, P.; Sautet, P. Molecular Adsorption at Pt (111). How Accurate are DFT Functionals? *Phys. Chem. Chem. Phys.* **2015**, *17*, 28921–28930.
- (41) Henkelman, G.; Uberuaga, B. P.; Jonsson, H. A Climbing Image Nudged Elastic Band Method for Finding Saddle Points and Minimum Energy Paths. *J. Chem. Phys.* **2000**, *113*, 9901–9904.
- (42) Horiuti, I.; Polanyi, M. Exchange Reactions of Hydrogen on Metallic Catalysts. *Trans. Faraday Soc.* **1934**, *30*, 1164–1172.
- (43) Zhao, Z.-J.; Chiu, C.-c.; Gong, J. Molecular Understandings on the Activation of Light Hydrocarbons over Heterogeneous Catalysts. *Chem. Sci.* **2015**, *6*, 4403–4425.
- (44) Lillehaug, S.; Børve, J.; Sierka, M.; Sauer, J. Catalytic Dehydrogenation of Ethane over Mononuclear Cr(III) Surface Sites on Silica. part I. C–H Activation by  $\sigma$ -Bond Metathesis. *J. Phys. Org. Chem.* **2004**, *17*, 990–1006.
- (45) Carrà, S.; Forni, L.; Vintani, C. Kinetics and Mechanism in Catalytic Dehydrogenation of n-butane over Chromia-Alumina. *J. Catal.* **1967**, *9*, 154–165.
- (46) Wischert, R.; Copéret, C.; Delbecq, F.; Sautet, P. Optimal Water Coverage on Alumina: A Key to Generate Lewis Acid–Base Pairs that are Reactive Towards the C–H Bond Activation of Methane. *Angew. Chem., Int. Ed.* **2011**, *50*, 3202–3205.
- (47) Wischert, R.; Laurent, P.; Copéret, C.; Delbecq, F.; Sautet, P.  $\gamma$ -Alumina: The Essential and Unexpected Role of Water for the Structure, Stability, and Reactivity of “Defect” Sites. *J. Am. Chem. Soc.* **2012**, *134*, 14430–14449.
- (48) Kozuch, S.; Shaik, S. How to Conceptualize Catalytic Cycles? The Energetic Span Model. *Acc. Chem. Res.* **2011**, *44*, 101–110.